Joint UAV Position and Power Optimization for Accurate Regional Localization in Space-Air Integrated Localization Network

Yue Zhao, *Member, IEEE*, Zan Li, *Senior Member, IEEE*, Nan Cheng, *Member, IEEE*, Benjian Hao, *Member, IEEE*, and Xuemin Shen, *Fellow, IEEE*

***Abstract*—Accurate location estimation of Internet-of-Things (IoT) devices within an Area of Interest (AoI) is a challenging issue, especially in a global navigation satellite system (GNSS)-constrained environment. In this article, we present a space-air integrated localization network (SAILN) architecture to exploit the advantages of the unmanned-aerial-vehicle (UAV)-based localization through joint position and power optimization (JPPO) strategies. In SAILN, UAVs can utilize their flexible movement to obtain the line-of-sight (LOS) path with a high probability, thereby providing the potential IoT devices in the AoI with supplementary localization information. The JPPO of UAVs aims to improve the regional localization accuracy for the entire AoI, considering the no-fly-zone (NFZ) and the total energy constraint. We propose the average localization accuracy increment (ALAI) of the sampling points in the AoI as the metric to measure the performance of SAILN compared with that of only satellites, which is regarded as the objective to formulate the JPPO problems for UAV operations in both static and dynamic SAILN. The intractable problems can be resolved by the pure genetic algorithm (PGA) that has a low computational cost and unique features suiting the JPPO of UAVs. Then, by taking advantage of the ALAI convexity to the UAVs' power, we propose a power reallocation-based two-step algorithm (PRTSA) to further explore an improved JPPO solution. Simulation results validate that the proposed PRTSA can obtain a higher localization accuracy for the entire AoI than the PGA and the other straightforward baselines.**

***Index Terms*—Area of Interest (AoI), deployment and trajectory design, localization, power allocation, unmanned aerial vehicle (UAV).**

I. Introduction

With the rapid development of Internet of Things (IoT), a myriad of location-based services have emerged, such as autonomous driving, smart cities, industrial automation, and so forth [1]–[4]. These applications are supported by the extremely accurate location information of IoT devices deployed in the based terrain. Currently, the commonly used localization platform is the global navigation satellite system (GNSS), which can provide the localization accuracy of the order of meters [5], based on the code-based and the phase-based observations. However, satellite-based localization systems may be incapable of providing enough accuracy for IoT devices under certain adverse conditions, such as urban canyons and flyovers, since obstacles or lousy weather conditions very likely block the satellite signals [6], [7]. Hence, enhanced or brand-new localization platforms are indispensable to meet the increasing demand for accurate location in harsh scenes to better provide location-based services to multiple potential IoT devices in the Area of Interest (AoI). Compared with satellites, the advantage of the unmanned aerial vehicle (UAV) is their adjustable altitude, power, and mobility [8], [9]. As a promising paradigm, space-air-ground integrated network (SAGIN) has recently attracted intensive research interests by integrating UAVs' merits and connecting the aerial platforms with current satellite network [10]–[12].

With SAGIN, UAVs can be regarded as supplementary localization nodes transmitting radio frequency signals to help potential IoT devices in the AoI determine their positions [13], and form the space-air integrated localization network (SAILN) with satellites. There are two types of network localization nodes (NLNs) in SAILN, i.e., satellites and UAVs, providing different functionalities decided by their characteristics. Thus, it is imperative to exploit the specific advantages of each networking paradigm. The satellites can provide broad coverage and always-on services for IoT devices through seamless coverage [12], [14]. In many promising fields, e.g., intelligent transportation system and disaster rescue, the IoT devices are clustered in a specific AoI to execute certain applications. Due to the lack of focus of satellites' signals, the localization accuracy of IoT devices in the AoI fails to meet the requirement. In this case, the UAVs can hover on top of the AoI to offer extra localization information for a regional basis by reaping their higher signal-to-noise ratio (SNR) and line-of-sight (LOS) probability [15]–[17].

The localization accuracy for potential IoT devices in the AoI depends on the network geometry of NLNs and receivers, transmit power and waveforms of NLNs' signals, and the conditions of transmission channels, and so forth [6]. Therefore,

Manuscript received May 3, 2020; revised July 31, 2020 and October 1, 2020; accepted October 5, 2020. Date of publication October 12, 2020; date of current version March 5, 2021. This work was supported in part by the National Natural Science Foundation of China under Grant 61825104 and Grant 61631015; in part by the China Scholarship Council; and in part by the Natural Sciences and Engineering Research Council of Canada. *(Corresponding author: Yue Zhao.)*

Yue Zhao, Zan Li, Nan Cheng, and Benjian Hao are with the State Key Laboratory of Integrated Services Networks, School of Telecom. Engineering, Xidian University, Xi'an 710071, China (e-mail: yuezhao@xidian.edu.cn; zanli@xidian.edu.cn; dr.nan.cheng@ieee.org; bjhao@xidian.edu.cn).

Xuemin Shen is with the Department of Electrical and Computer Engineering, University of Waterloo, Waterloo, ON N2L 3G1, Canada (e-mail: sshen@uwaterloo.ca).

Digital Object Identifier 10.1109/JIOT.2020.3030064

the spatial positions and transmit power of NLNs have a significant impact on the localization accuracy. In particular, the localization accuracy improvement for the IoT devices in the AoI mainly hinges on deploying the operable UAVs, i.e., height, direction, and power. On one hand, compared with satellites whose orbits and schedules are preset and cannot be changed arbitrarily, the 3-D positions of UAVs are adjustable to accommodate diverse environments and form advantageous network geometries. On the other hand, the power levels of UAVs' transmitted signals can be matched with their positions to optimize the localization precision for the IoT devices. From the interference point of view, the total power of all the UAVs is constrained. In addition, each UAV carries limited onboard energy during a finite flight period [18], so that the maximum available power to broadcast signal is bounded. Consequently, UAV operation strategy, i.e., joint position and power optimization (JPPO), is worth investigating in SAILN to improve the localization accuracy for the AoI with the constraint of energy consumption.

NLN operations have been widely investigated in recent literature [19]–[24]. Most NLN operation strategies focused on optimizing the position and power of NLNs separately, or analyzing the localization geometry but ignoring the constraints of the actual deployment area and the total available power, or only providing the NLN operations for a single user. Shen and Win [19] and Win *et al.* [20] proposed three network operation strategies, i.e., node prioritization, node activation, and node deployment to improve localization performance and energy efficiency. Specifically, the NLN deployment in 2-D time of arrival (TOA)-based localization scenario was studied in [19], and was solved by deriving the geometric interpretation of eigenvalues of the localization information matrix. In [20], the NLNs' power optimization problem was formulated by exploring the functional properties of the localization accuracy metric and was transformed into second-order cone programs for solving. However, the algorithms mentioned above may not be easily implemented in 3-D JPPO of UAVs owing to the intractable mathematical analysis of the Fisher information matrix (FIM), a complicated combination of azimuth angle, elevation angle, distance, and power. Yang *et al.* [21], [22] proposed the NLN deployment strategies in 2-D and 3-D time difference of arrival (TDOA)-based localization by finding a lower value of Cramér Rao bound (CRB) and determining the corresponding equality condition. The equality condition can only be achieved when the network follows a uniform angular array, giving a fixed result and placing NLNs around the user or the target. Nguyen and Doğançay [23] proposed the deployment solution for 2-D TOA-based localization by minimizing the area of estimation confidence region and the optimal deployment strategy was determined by a group of specific angles. Xu and Doğançay [24] proposed a deployment method for 3-D Angle-of-Arrival (AOA)-based localization by analyzing the trigonometric relationship of angles to reach a minimum available CRB. However, these methods may not be applied to UAV deployment in 3-D SAILN scenario since the irregular deployment area is unavoidable and the optimal angles are not attained. The aforementioned works in the context of NLN operations [19]–[24] only concentrated on a single source or user, so that their frameworks cannot be applied directly to 3-D SAILN, which dedicates to providing broad coverage and localization services for the potential multiple IoT devices in the AoI. Besides, a feature of UAV-based localization is the existence of LOS transmission with a high probability, which is beneficial for TOA-based localization [6], [25]. Thus, except for the localization geometry, it is indispensable to consider the special effect of the elevation angle between the UAVs and the potential IoT devices in the AoI on the LOS path probability, which depends on the widely studied drone-to-ground (D2G) channel model [26].

In this article, we investigate the JPPO of UAVs in SAILN to minimize the localization error for the entire AoI, which is equivalent to maximize the average localization accuracy increment (ALAI) of sampling points in the AoI when UAVs are added into formerly existing satellites network. Specifically, we formulate the JPPO problems in both static and dynamic SAILNs subject to the deployment area and power constraints. The JPPO problems are intractable to derive an analytical closed-form solution due to the nonconvex and implicit mathematical connection between the objective and the decision variables. By customizing the nature-inspired metaheuristic algorithm into the JPPO problems, a pure genetic algorithm (PGA) is proposed. To be specific, the transmit powers and positions of UAVs are integrated into an independent vector, and the optimal solution can be approached with several iteratively evolutionary cycles. However, an expected drawback of the PGA is that the power may be far from the optimal values due to the large gap between transmit power levels, e.g., a few watts and location scale, e.g., several kilometers. To further improve the JPPO solution obtained by the PGA, a power reallocation-based two-step algorithm (PRTSA) is proposed to reallocate the UAVs' power by using the convex optimization technique. Simulation results validate that the PGA and the PRTSA can obtain solutions without violating constraints and determine better UAV operations solutions than three straightforward baseline methods. Besides, simulations reveal that the proposed PRTSA is robust in the presence of the UAVs' position uncertainties. The main contributions of this article can be summarized as follows.

1) We provide a JPPO framework of UAVs in SAILN to seek optimal allocated power and deployed positions of UAVs, thereby improving the localization accuracy for the entire AoI with potential IoT devices.
2) We define ALAI as the localization accuracy metric of the AoI when extra UAVs are added into the original satellite network. Then, in both static and dynamic SAILNs, the JPPO problems are formulated to maximize the ALAI subject to UAVs' deployment area and power constraints.
3) We propose the PGA and the PRTSA to solve the intractable JPPO problems. Specifically, the PGA can obtain the candidate solution of the original JPPO problems. Then, the candidate solution can be improved by the PRTSA, which makes use of the convex optimization technique to reallocate the power of UAVs further.

The remainder of this article is organized as follows. Section II describes the system model, and Section III gives the

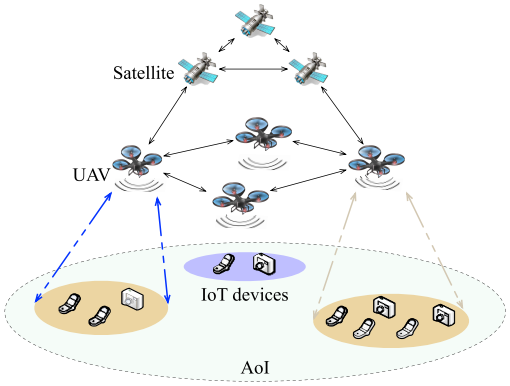

Fig. 1. Overview of the SAILN.

localization accuracy metrics. In Section IV, the JPPO problems are formulated and analyzed. Optimization algorithms are proposed in Section V. Section VI presents the simulation results and discussions. Finally, Section VII concludes this article and gives the future work.

II. System Model

A. Network Settings

We consider a ground AoI where IoT devices are deployed to conduct certain tasks with the exact position requirement. In the AoI, the signals transmitted from satellites are blocked or disturbed so that a SAILN is introduced to provide localization supports. The overview of the conceived network is shown in Fig. 1. The spatial satellites and aerial UAVs in SAILN can propagate localization signals containing their positions and transmit time. The UAVs' positions can be derived by receiving the satellites' signals and the assistance of ground base stations. Meanwhile, all the UAVs are managed by the controller of the SAILN to achieve unified scheduling. In the ground AoI, there are several IoT devices, either clustered together or dispersed, and each of them independently measures the TOAs of the NLNs' signals and then calculates distances. Note that, the transmissions between UAVs and satellites are continuous because of the parametric stabilization space-air channels. To facilitate the theoretical analysis in this article, we also assume that the transmission outage is absent when the IoT devices receive the NLNs' localization signal.

In SAILN, the sets of satellites and UAVs are represented by $\mathcal{N}_s = \{1, 2, \ldots, N_s\}$ and $\mathcal{N}_u = \{1, 2, \ldots, N_u\}$, respectively. For convenient analysis, the positions of the participants in SAILN are defined in a conventional coordinate system, which means the X-Y plane is regarded as the ground and the z-axis denotes the height. Thus, in a static SAILN, the position of ith satellite in $\mathcal{N}_s$ is denoted by $\boldsymbol{s}_i = (s_{x,i}, s_{y,i}, s_{z,i})^T$ and the position of jth UAV in $\mathcal{N}_u$ is given by $\boldsymbol{u}_j = (u_{x,j}, u_{y,j}, u_{z,j})^T$. The position of the potential IoT device in the AoI $\mathcal{A}$ is $\boldsymbol{a} = (a_x, a_y, a_z)^T$. We define $\boldsymbol{P} = [P_1, P_2, \ldots, P_{N_u}]$ and $\boldsymbol{U} = [\boldsymbol{u}_1^T, \boldsymbol{u}_2^T, \ldots, \boldsymbol{u}_{N_u}^T]$ as the set of allocated power values and the set of deployed positions of UAVs, respectively. Moreover, we consider a dynamic SAILN within a period T, which can be divided into N_t slots with equal duration δ_t [26]. The dynamic network is an extension of the static network and can be regarded as a combination of many consecutive static networks in the time domain. The set of time slots is represented by $\mathcal{N}_t = \{1, 2, \ldots, N_t\}$. At time step $t \in \mathcal{N}_t$, the positions of satellites and UAVs can be modified as $\boldsymbol{s}_i[t] = (s_{x,i}[t], s_{y,i}[t], s_{z,i}[t])^T$ and $\boldsymbol{u}_j[t] = (u_{x,j}[t], u_{y,j}[t], u_{z,j}[t])^T$, respectively. Vector $\boldsymbol{P}[t] = \{P_1[t], P_2[t], \ldots, P_{N_u}[t]\}$ and matrix $\boldsymbol{U}[t] = \{\boldsymbol{u}_1[t], \boldsymbol{u}_2[t], \ldots, \boldsymbol{u}_{N_u}[t]\}^T$ are used to represent the power allocation strategy and positions of UAVs over the entire time period, respectively. The AoI also changes over time, i.e., $\mathcal{A}[t]$, which should be known by the SAILN from the perspective of network design.

B. Ranging Information

In SAILN, the IoT device calculates its position by estimating the TOAs of the radio frequency signal transmitted from NLNs. We assume that the UAVs and the ground users are synchronous by receiving satellites' signal. For example, the global positioning system (GPS) can be used for clock synchronization with an accuracy of ten nanoseconds [27], [28]. The parameter to measure the contribution of each NLN to the localization accuracy is the ranging information. Next, the UAV $\boldsymbol{u}_j$ and a potential IoT device $\boldsymbol{a}_k = (a_{x,k}, a_{y,k}, a_{z,k})^T$ in the AoI are used to reveal the effect of transmission channel and geometric relationship on the ranging information.

The actual TOA between $\boldsymbol{u}_j$ and $\boldsymbol{a}_k$ is

$$t_{j,k} = \frac{d_{j,k}}{c} = \frac{1}{c}\left\|\boldsymbol{u}_j - \boldsymbol{a}_k\right\|_2 \tag{1}$$

where $\|\cdot\|_2$ is the Euclidean norm, c is the speed of the signal, and $d_{j,k}$ is the distance between $\boldsymbol{u}_j$ and $\boldsymbol{a}_k$. The azimuth angle $\theta_{j,k}$ and elevation angle $\phi_{j,k}$ are in nonlinear manner as

$$\theta_{j,k} = \arctan\left(\frac{u_{y,j} - a_{y,k}}{u_{x,j} - a_{x,k}}\right) \tag{2}$$

$$\phi_{j,k} = \arctan\left(\frac{u_{z,j} - a_{z,k}}{\sqrt{\left(u_{x,j} - a_{x,k}\right)^2 + \left(u_{y,j} - a_{y,k}\right)^2}}\right). \tag{3}$$

The ranging information is a matrix, defined in [6] as

$$\boldsymbol{J}_{j,k}(\boldsymbol{a}_k) = \mu_{j,k}\boldsymbol{q}_{j,k}\boldsymbol{q}_{j,k}^T. \tag{4}$$

On one hand, $\boldsymbol{q}_{j,k}$ is a unit direction vector and is only related to angles between the IoT device $\boldsymbol{a}_k$ and the UAV $\boldsymbol{u}_j$

$$\boldsymbol{q}_{j,k} = \left(\cos\phi_{j,k}\cos\theta_{j,k},\ \cos\phi_{j,k}\sin\theta_{j,k},\ \sin\phi_{j,k}\right)^T. \tag{5}$$

On the other hand, $\mu_{j,k}$ is a nonnegative scalar called as the ranging information intensity (RII) which is related to the characteristics of signals and transmission channels [6], [19].

With actual multipath scenario, we assume that the transmission between UAVs and IoT devices contains LOS path with a high probability [18], because only the LOS signal is beneficial for improving localization accuracy [6]. Thus, after separating the parameters related to distance and elevation angle, RII $\mu_{j,k}$ can be expressed as

$$\mu_{j,k} \propto \phi_{j,k}\frac{P_j}{d_{j,k}^2} = \xi \cdot \frac{u_{z,j}}{\sqrt{d_{j,k}^2 - u_{z,j}^2}}\frac{P_j}{d_{j,k}^2} \tag{6}$$

where ξ is a nonnegative scalar related to the multipath propagation property and the effective bandwidth of transmitted signal but independent with distance $d_{j,k}$ and transmit power P_j of the UAV $\boldsymbol{u}_j$. From the perspective of network design, we assume that ξ is fixed throughout the entire AoI, which can be inferred by the controller of SAILN based on the historical statistics. In (6), $\mu_{j,k}$ is proportional to $\phi_{j,k}$ to reflect the large-scale fading, which can be derived from the D2G channel [26]. Therefore, we have the observation from (6) that the ranging information provided by each UAV is determined by the UAV's power, UAV-IoT device distance, UAV-AoI channel status, and UAV-IoT device elevation angle.

III. Localization Accuracy Metrics

In this section, the metrics to measure the localization accuracy are discussed. We first focus on the SAILN with a single IoT device to derive the squared position error bound (SPEB). Then, the localization accuracy increment is explained when extra UAVs are added into the satellite network. The ALAI is then considered to be the metric to measure the JPPO for UAVs.

A. Squared Position Error Bound

In the noncooperative SAILN, TOAs of signals transmitted from satellites and UAVs are measured by the IoT devices independently. Therefore, TOA measurement errors are uncorrelated, and the localization information provided by different NLNs can be added directly. Shen and Win [6] defined the SPEB as the limit for the mean squared error (MSE) to evaluate the localization accuracy. Specifically, SPEB for the IoT device $\boldsymbol{a}_k$, i.e., $\mathcal{P}(\boldsymbol{a}_k)$, satisfies

$$\mathcal{P}(\boldsymbol{a}_k) \triangleq \mathrm{tr}\left\{(\boldsymbol{J}(\boldsymbol{a}_k))^{-1}\right\} \leq \mathbb{E}\left\{\left\|\hat{\boldsymbol{a}}_k - \boldsymbol{a}_k\right\|_2^2\right\} \tag{7}$$

where $\hat{\boldsymbol{a}}_k$ is the position estimation of $\boldsymbol{a}_k$ and $\mathrm{tr}\{\cdot\}$ denotes the matrix trace operator. $\boldsymbol{J}(\boldsymbol{a}_k)$ is the integrated equivalent FIM (IEFIM) provided by the SAILN, which consists of two parts, equivalent FIM (EFIM) provided by satellites and EFIM provided by UAVs

$$\begin{aligned}\boldsymbol{J}(\boldsymbol{a}_k) &= \boldsymbol{J}_s(\boldsymbol{a}_k) + \boldsymbol{J}_u(\boldsymbol{a}_k) \\ &= \sum_{i\in\mathcal{N}_s} \boldsymbol{J}_{i,k}(\boldsymbol{a}_k) + \sum_{j\in\mathcal{N}_u} \boldsymbol{J}_{j,k}(\boldsymbol{a}_k)\end{aligned} \tag{8}$$

where $\boldsymbol{J}_{i,k}(\boldsymbol{a}_k)$ and $\boldsymbol{J}_{j,k}(\boldsymbol{a}_k)$ are ranging information matrices provided by satellite $\boldsymbol{s}_i$ and UAV $\boldsymbol{u}_j$, respectively.

B. Statistical Metric for the Entire AoI

It has been proved that the localization accuracy improves when an extra NLN is added into the network [29]. Namely, the UAV's additional localization information is beneficial for reducing the localization error of the IoT devices. Thus, for a potential IoT device in the AoI, e.g., $\boldsymbol{a}_k$, we have

$$\Delta\mathcal{P}(\boldsymbol{a}_k) \triangleq \mathcal{P}_s(\boldsymbol{a}_k) - \mathcal{P}(\boldsymbol{a}_k) > 0 \tag{9}$$

where $\mathcal{P}_s(\boldsymbol{a}_k) = \mathrm{tr}\{(\boldsymbol{J}_s(\boldsymbol{a}_k))^{-1}\}$ is the SPEB determined by satellites and $\mathcal{P}(\boldsymbol{a}_k) = \mathrm{tr}\{(\boldsymbol{J}_s(\boldsymbol{a}_k)+\boldsymbol{J}_u(\boldsymbol{a}_k))^{-1}\}$ is a lower SPEB determined by satellites and extra UAVs.

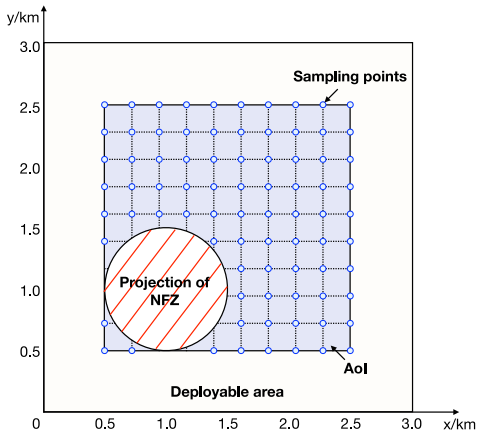

Fig. 2. Two dimensional illustration of the AoI and NFZ.

According to the above analysis, for the potential IoT device $\boldsymbol{a}_k$ in the AoI, N_u UAVs can be deployed to maximize the accuracy increment $\Delta\mathcal{P}(\boldsymbol{a}_k)$. However, such a deployment strategy is unfair to other potential IoT devices in the AoI. A specific parameter is desired to reflect the localization increment of the entire AoI.

We divide the entire AoI as many subareas to obtain N_k sampling points, as shown in Fig. 2. The position of the kth sampling point is denoted by

$$\boldsymbol{a}_k = \left(a_{x,k}, a_{y,k}, a_{z,k}\right)^T, \quad k \in \mathcal{N}_k \tag{10}$$

where $\mathcal{N}_k = \{1, 2, \ldots, N_k\}$.

Generally, for a small area, the SPEBs of the sampling points provided by satellites are at the same level, so that the accuracy increment $\Delta\mathcal{P}(\boldsymbol{a}_k)$ for all the sampling points is quite similar. Therefore, in this article, we can use the ALAI to measure the performance of SAILN for the entire AoI. Specifically, the ALAI $\mathcal{P}^A$ is defined as

$$\mathcal{P}^A = \frac{1}{N_k}\sum_{k=1}^{N_k} \Delta\mathcal{P}(\boldsymbol{a}_k). \tag{11}$$

IV. JPPO Problem Formulations

The concerned SAILN is a typical partially controllable network that the positions and orbits of satellites are fixed and preset. Thus, the goal of the JPPO of UAVs is to find the optimal deployed positions and allocated power values of UAVs to improve the localization accuracy of the entire AoI as much as possible. In this section, the JPPO problem in the static SAILN is first formulated, which is then extended to a dynamic SAILN with multiple time slots.

A. Problem Formulation in Static SAILN

In a static network, the JPPO problem is formulated as

$$\mathscr{P}^{\mathrm{S}}: \underset{\boldsymbol{P},\boldsymbol{U}}{\text{maximize}} \quad \mathcal{P}^A \tag{12}$$

$$\text{s.t.} \quad \text{C1: } \boldsymbol{u}_j \in \mathcal{D} \quad \forall j \in \mathcal{N}_u, \tag{13}$$

$$\text{C2: } \left\|\boldsymbol{u}_i - \boldsymbol{u}_j\right\|_2 \geq s_{\min} \quad \forall i, j \in \mathcal{N}_u, i \neq j \tag{14}$$

$$\text{C3: } 0 \le P_j \le P_{\max} \quad \forall j \in \mathcal{N}_u \tag{15}$$

$$\text{C4: } \sum_{j=1}^{\mathcal{N}_u} P_j \le P_{\text{total}}. \tag{16}$$

The ALAI $\mathcal{P}^A$ of the sampling points in the AoI is regarded as the objective. Constraint C1 limits the deployment area of UAVs, which may be irregular in an actual environment determined by the building obstacles and communication range, etc. We assume that the deployment area is larger than the AoI. Constraint C2 is to avoid spatial collision of UAVs, namely, the distance between any two UAVs cannot be smaller than a predefined safe distance $s_{\min}$. Constraint C3 guarantees the power constraint for each UAV with a maximum allowable transmit power $P_{\max}$. Constraint C4 gives the total available power P_{total}, which is the upper bound of the sum of all the UAVs' power. Note that, in $\mathscr{P}^{\text{S}}$, the number of deployed UAVs N_u should be known in advance, because the dimension of variables is the essence when solving the problem.

B. Problem Formulation in SAILN With Multiple Time Slots

We then extend the JPPO problem to a dynamic SAILN with multiple time slots. It is assumed that the UAVs can accurately move to the position obtained from the previous moment. Due to the moving speed constraint $v_{u,\max}$, the position shift of each UAV within two continuous time slots cannot exceed the maximum distance constraint, i.e.,

$$\text{C5}: \left\|\boldsymbol{u}_j[t] - \boldsymbol{u}_j[t-1]\right\|_2 \le v_{u,\max}\delta_t \quad \forall j \quad \forall t. \tag{17}$$

Thus, according to changeable AoI $\mathcal{A}[t]$ at each time slot, the ALAI of sampling points in the current AoI $\mathcal{A}[t]$ is regarded as the objective and the one-step optimization problem at time step t can be formulated as

$$\mathscr{P}^{\text{MT}}: \underset{\boldsymbol{P}[t],\boldsymbol{U}[t]}{\text{maximize}} \ \mathcal{P}^A[t] \quad \text{s.t.} \quad \text{C1}-\text{C5}. \tag{18}$$

V. Optimization Algorithms

The formulated JPPO problems $\mathscr{P}^S$ and $\mathscr{P}^{\text{MT}}$ are nonconvex, where the nonconvexity mainly arises from the relationship between positions of UAVs and localization accuracy metrics. Besides, the irregular deployment areas in C1 and Euclidean norms in C2 and C5 also make the optimization problems complicated and intractable, so that it is challenging to solve the formulated problems optimally by the analytically mathematical deductions. Based on the nature-inspired metaheuristic algorithms, we customize a PGA, i.e., PGA, to address these NP-hard problems. To get closer to the optimal solution, we propose the PRTSA to reallocate UAVs' powers by formulating a convex optimization problem. In this section, the genetic algorithm is introduced first, and the PRTSA is provided after the JPPO problem is transformed.

A. Genetic Algorithm

Genetic algorithm is a well suited and capable numerical-approach to address nonconvex and nonlinear optimization problems in plenty of practical engineering problems, e.g., mesh network planning [30] and traffic scheduling [31], which are always challenging to derive an analytically mathematical solution. Meanwhile, the genetic algorithm can converge rapidly and can be implemented on digital signal processors (DSPs) and FPGA [32].

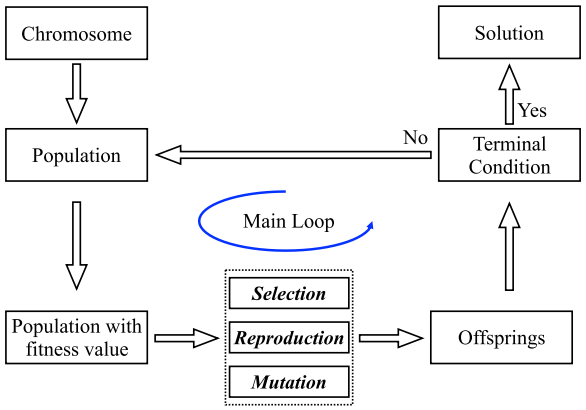

Fig. 3. Procedures of the genetic algorithm.

The flow chart of the genetic algorithm is shown in Fig. 3. The genetic algorithm starts to abstract the representations of decision variables as genes and strings them together into a chromosome. An initial population consists of many individuals, and each individual has a specific fitness value concerning the optimization objective. Through biologically inspired operations, in offspring, more energetic individuals with larger fitness values are likely to survive while weaker individuals are more likely to be discarded [30]. After several evolutionary cycles, the fitness level throughout the population will improve. The individual with the largest fitness value will be selected and decoded as the solution of the original optimization problem when the terminal condition is attained.

B. PGA for the JPPO Problem $\mathscr{P}^S$

We then introduce the main procedures of solving $\mathscr{P}^{\text{S}}$ by using the PGA. In this article, we use only one chromosome to characterize the genotype of each individual. The allocated power values and deployed positions of UAVs are regarded as genes which are then strung together into a chromosome, i.e.,

$$\boldsymbol{\mathcal{X}} = \{\boldsymbol{P}, \boldsymbol{U}\} = \left\{ \underbrace{\overbrace{P_1, P_2, \ldots, P_{N_u}}^{N_u}, \overbrace{\boldsymbol{u}_1^T, \boldsymbol{u}_2^T, \ldots, \boldsymbol{u}_{N_u}^T}^{3\times N_u}}_{4\times N_u} \right\} \tag{19}$$

where $\boldsymbol{P}$ and $\boldsymbol{U}$ can be regarded as two genes.

1) Initial Population: The initial population $\mathfrak{X}^g$ consists of many individuals, i.e., $\mathfrak{X}^g = \{\boldsymbol{\mathcal{X}}_1^g, \boldsymbol{\mathcal{X}}_2^g, \ldots, \boldsymbol{\mathcal{X}}_{N_p}^g\}$, where the superscript g denotes the number of generation and N_p is the population size. The chromosome of each individual in $\mathfrak{X}^g$ is randomly generated within the feasible set, e.g., the pth chromosome in $\mathfrak{X}^g$ is $\boldsymbol{\mathcal{X}}_p^g = \{P_1, P_2, \ldots, P_{N_u}, \boldsymbol{u}_1^T, \boldsymbol{u}_2^T, \ldots, \boldsymbol{u}_{N_u}^T\}$, where $P_i \in [0, P_{\max}]$ and $\boldsymbol{u}_i \in \mathcal{D}\ \forall i \in \mathcal{N}_u$.

2) Evaluate Fitness: Fitness is associated with the objective function and all the constraints of the optimization problem and reflects the degree of goodness that individuals are suitable for solving the problem. Generally, individuals with

better fitness scores have a higher probability of surviving to reproduce offspring.

Because of the presence of constraints in $\mathscr{P}^{\mathrm{S}}$, the penalty function approach is reaping to filter the feasible solutions. With the constraint handling method proposed in [33] and [34], the fitness value of every chromosome is related to the objective function value and constraint violation. For instance, by decoding the chromosome $\boldsymbol{\mathcal{X}}_p^g$ as the powers and positions of UAVs, and substituting it into the definition of $\mathcal{P}^A$ in (11), the objective function value of pth chromosome in $\mathfrak{X}^g$ can be obtained

$$f\left(\boldsymbol{\mathcal{X}}_p^g\right) = \mathcal{P}^A|_{\boldsymbol{P}=\boldsymbol{\mathcal{X}}_p^g(1\,:\,N_u),\boldsymbol{U}=\boldsymbol{\mathcal{X}}_p^g(N_u+1\,:\,4N_u)}. \tag{20}$$

If the chromosome $\boldsymbol{\mathcal{X}}_p^g$ is feasible, its fitness function value is equal to the objective function value. On the contrary, if the chromosome $\boldsymbol{\mathcal{X}}_p^g$ is infeasible, similar with [33], its fitness function value is the objective function value of the worst feasible solution in the population, minus a sum of the constraint violations of the chromosome. The above operation avoids setting a penalty parameter and guarantees that the one having a smaller constraint violation is preserved when two infeasible solutions have a tournament selection. Mathematically, the fitness value can be obtained by

$$F\left(\boldsymbol{\mathcal{X}}_p^g\right) = \begin{cases} f\left(\boldsymbol{\mathcal{X}}_p^g\right), & \text{if } c_q\left(\boldsymbol{\mathcal{X}}_p^g\right) \geq 0 \quad \forall q = 1, 2, \ldots, N_q \\ f_{\min} - \sum_{q=1}^{N_q} \left\| c_q\left(\boldsymbol{\mathcal{X}}_p^g\right) \right\|, & \text{otherwise} \end{cases} \tag{21}$$

where $c_q(\boldsymbol{\mathcal{X}}_p^g), q = 1, 2, \ldots, N_q$ is the constraint violation of C2 and C4 in $\mathscr{P}^{\mathrm{S}}$, $N_q = \mathrm{C}_{N_u}^2 + N_u$, $\mathrm{C}_{N_u}^2$ is the number of combinations, $\|c_q(\boldsymbol{\mathcal{X}}_p^g)\|$ denotes the absolute value of the operand, and $f_{\min}$ is the objective function value of the worst feasible solution in the population. Specifically, if $q \leq \mathrm{C}_{N_u}^2$, we have $c_q(\boldsymbol{\mathcal{X}}_p^g) = \|\boldsymbol{u}_i - \boldsymbol{u}_j\|_2 - s_{\min}\ \forall i, j \in \mathcal{N}_u, i \neq j$; otherwise, we have $c_q(\boldsymbol{\mathcal{X}}_p^g) = P_{\text{total}} - \sum_{j=1}^{\mathcal{N}_u} P_j\ \forall j \in \mathcal{N}_u$.

Note that, C1 and C3 give the bound of the decision variables. If we consider a cylindrical no-fly-zone (NFZ), as shown in Fig. 2, we need add an extra constraint violation as $c_q(\boldsymbol{\mathcal{X}}_p^g) = \|\tilde{\boldsymbol{o}} - \tilde{\boldsymbol{u}}_j\|_2 - \tilde{r}\ \forall j \in \mathcal{N}_u$, where $\tilde{\boldsymbol{o}}$, $\tilde{\boldsymbol{u}}_j$, and $\tilde{r}$ are the center of the ground projection of the NFZ, the ground projection of $\boldsymbol{u}_j$, and the radius of the circular projection, respectively.

3) Selection: According to the predefined rules, the chromosomes in the current population ($\mathfrak{X}^g$) need to be handled by the selection operation, choosing parents for the next generation. Superior individuals tend to be preserved while the inferior individuals may be discarded. There are many manners to implement selection, e.g., proportionate selection, ranking, and tournament selection [35]. Specifically, Roulette wheel selection can select individuals proportionally according to their fitness values [30], while tournament selection involves several competitions among a few individuals chosen randomly from the population and determines the winner who has the largest fitness. In this article, the binary tournament selection is used since it can be in conjunction with the constraint handling method proposed in [33]. For example, when two chromosomes $\boldsymbol{\mathcal{X}}_{p1}^g$ and $\boldsymbol{\mathcal{X}}_{p2}^g$ compete, if $F(\boldsymbol{\mathcal{X}}_{p1}^g) > F(\boldsymbol{\mathcal{X}}_{p2}^g)$, then the chromosome $\boldsymbol{\mathcal{X}}_{p1}^g$ is retained and $\boldsymbol{\mathcal{X}}_{p2}^g$ is abandoned.

Algorithm 1: PGA for the JPPO Problem $\mathscr{P}^S$

Input: The positions of satellites $\boldsymbol{s}_i,\ \forall \in \mathcal{N}_s$, the deployable area $\mathcal{D}$, the AoI $\mathcal{A}$, the UAV-AoI channel parameter ξ, the total available power P_{total}, the maximum available power for each UAV $P_{\max}$, the safe distance $s_{\min}$, the number of generation g, and the maximum number of generations N_g.

Output: The deployed positions and allocated power values of UAVs, i.e., $\boldsymbol{U}^c$ and $\boldsymbol{P}^c$.

```
g ← 1;
Initialize the population 𝔛^g with N_p individuals, i.e., 𝔛^g = {X_1^g, X_2^g, ..., X_{N_p}^g};
Calculate fitness of all the individuals based on (21), F(X_p^g), p = 1, 2, ..., N_p;
Record chromosome with the maximum fitness as X^c = argmax(F(X_p^g)), p = 1, 2, ..., N_p;
while g < N_g do
    Apply tournament selection to select parents for next generation;
    Reserve elites and apply crossover to selected parents to generate children remaining feasible;
    Apply mutation to newly generated children remaining feasible;
    Calculate fitness and update the best chromosome;
end
Decode the best chromosome X^c as U^c and P^c.
```

4) Reproduction: Reproduction dedicates to creating offspring due to the lack of individuals in the population caused by selection. To preserve good genes and make them appeared frequently, the reproduction consists of elite reservation and crossover to make up the number of individuals lost in the previous step to the original population size. A set of elites ($\mathfrak{X}_{\text{elite}}^g$) with larger fitness is retained directly to the next population. Meanwhile, the other chromosomes in the set $\mathfrak{X}^g - \mathfrak{X}_{\text{elite}}^g$ are processed by the intermediate crossover, which creates the offspring by taking a weighted average of the parents. For instance, the offspring's chromosome of two individuals with chromosomes $\boldsymbol{\mathcal{X}}_{p1}^g$ and $\boldsymbol{\mathcal{X}}_{p2}^g$ is

$$\boldsymbol{\mathcal{X}}_{p1}^g + \boldsymbol{l} \odot \left(\boldsymbol{\mathcal{X}}_{p2}^g - \boldsymbol{\mathcal{X}}_{p1}^g\right) \tag{22}$$

where vector $\boldsymbol{l}$ follows uniform distribution $U(0, 1)$, and $\odot$ represents the Schur product, i.e., element-by-element multiplication.

5) Mutation: The mutation operation is to generate desirable characterization of the gene to bring solutions out of local optimal points [30]. The adaptive feasible mutation manner can randomly generate directions that are adaptive to the last successful or unsuccessful generation and can choose a direction and step length that satisfies bounds and linear constraints, i.e., C1 and C3 in $\mathscr{P}^S$.

Algorithm 1 shows the details of the proposed PGA for solving $\mathscr{P}^S$. Note that, the terminal condition of the PGA is when the maximum number of generations is attained.

Algorithm 2: PRTSA for the JPPO Problem $\mathscr{P}^S$

Input: The inputs are the same as Algorithm 1.
Output: The deployed positions and allocated power values of UAVs, i.e., $\boldsymbol{U}^c$ and $\boldsymbol{P}^*$.
1 Solve $\mathscr{P}^{\mathrm{S}}$ by using the PGA and obtain the candidate solution, $\boldsymbol{\mathcal{X}}^c = \{\boldsymbol{P}^c, \boldsymbol{U}^c\}$;
2 Discard $\boldsymbol{P}^c$ and Substitute $\boldsymbol{U}^c$ into $\mathscr{P}^{\mathrm{SP-R}}$, which is then solved by interior-point approach;
3 Obtain the improved solution $\boldsymbol{P}^*$ and $\boldsymbol{\mathcal{X}}^* = \{\boldsymbol{P}^*, \boldsymbol{U}^c\}$.

The above PGA treats the combination of the powers and the positions of UAVs as one chromosome in vector form, which brings additional dependency between the power and positions. However, there is a significant gap between the strength of the power and the level of 3-D position in practice. For instance, the transmit power of a UAV may be a few watts, while the coordinate of the UAV is several kilometers, which leads to that the power is sensitive to the errors. Besides, the formulation of a fitness function, the use of population size, the choice of parameters, such as the rate of mutation and crossover, all increase the probability that the PGA falling into local optima. To compensate for the candidate solution solved by the PGA, i.e., $\boldsymbol{\mathcal{X}}^c$, we try to improve the objective function value by optimizing the allocated power of UAVs in the next section.

C. PRTSA for the JPPO Problem $\mathscr{P}^S$

When $\boldsymbol{\mathcal{X}}^c$ is obtained, we can keep the position of the UAVs as $\boldsymbol{U}^c$ and use a convex optimization technique to resolve the following power reallocation problem:

$$\mathscr{P}^{\mathrm{SP}}: \underset{\boldsymbol{P}}{\text{maximize}} \quad \mathcal{P}^A \tag{23}$$

$$\text{s.t.} \quad \text{C3: } 0 \le P_j \le P_{\max} \ \forall j \in \mathcal{N}_u \tag{24}$$

$$\text{C4: } \sum_{i=1}^{\mathcal{N}_u} P_j \le P_{\text{total}} \tag{25}$$

$$\text{C6: } \boldsymbol{U} = \boldsymbol{U}^c \tag{26}$$

where only C3 and C4 are retained compared with $\mathscr{P}^S$. Constraint C6 denotes that the position of UAVs equals the candidate solution solved by the PGA and is not optimized in $\mathscr{P}^{SP}$. Constraints C3 and C4 are convex with respect to the allocated power of UAVs.

We then transform the optimization problem $\mathscr{P}^{\mathrm{SP}}$ as a semidefinite program (SDP) and provide the explicit convexity relation of $\mathcal{P}^A$ concerning $\boldsymbol{P}$. From (11), the detailed expression of $\mathcal{P}^A$ can be given as

$$\mathcal{P}^A = \frac{1}{N_k}\sum_{k=1}^{N_k} \mathrm{tr}\Big\{ (\boldsymbol{J}_s(\boldsymbol{a}_k))^{-1} - (\boldsymbol{J}_s(\boldsymbol{a}_k) + \boldsymbol{J}_u(\boldsymbol{a}_k))^{-1} \Big\}. \tag{27}$$

We introduce N_k auxiliary matrices $\boldsymbol{Z}_k \ \forall k \in \mathcal{N}_k$, to relax the multiple inverse operations, which yields

$$\boldsymbol{Z}_k \preceq (\boldsymbol{J}_s(\boldsymbol{a}_k))^{-1} - (\boldsymbol{J}_s(\boldsymbol{a}_k) + \boldsymbol{J}_u(\boldsymbol{a}_k))^{-1} \tag{28}$$

Algorithm 3: PRTSA for the JPPO Problem $\mathscr{P}^{\mathrm{MT}}$

Input: The initial deployable area $\mathcal{D}$, the initial AoI $\mathcal{A}[1]$, the difference of AoI at adjacent time slot $\Delta\mathcal{A}$, the UAV-AoI channel parameter ξ, total available power P_{total}, the maximum available power for each UAV $P_{\max}$, the maximum speed $v_{u,\max}$, the safe distance $s_{\min}$, and satellite's positions $\boldsymbol{s}_i[t], \forall i \in \mathcal{N}_s, \forall t \in \mathcal{N}_t$.
Output: The deployed positions and allocated power values of UAVs at each time step, i.e., $\boldsymbol{U}^c[t], \boldsymbol{P}^*[t], \forall t \in \mathcal{N}_t$.
1 **while** $t \in \mathcal{N}_t$ **do**
2 Based on $\mathcal{D}$ and $\mathcal{A}[t]$, solve $\mathscr{P}^{\mathrm{MT}}$ by using the PGA and interior-point approach;
3 Obtain the solution $\boldsymbol{P}^*[t]$ at each time step and $\boldsymbol{\mathcal{X}}^*[t] = \{\boldsymbol{P}^*[t], \boldsymbol{U}^c[t]\}$;
4 $\mathcal{A}[t] = \mathcal{A}[t-1] + \Delta\mathcal{A}$;
5 **end**

which is equivalent to

$$(\boldsymbol{J}_s(\boldsymbol{a}_k))^{-1} - \boldsymbol{Z}_k - (\boldsymbol{J}_s(\boldsymbol{a}_k) + \boldsymbol{J}_u(\boldsymbol{a}_k))^{-1} \succeq \boldsymbol{0}. \tag{29}$$

We can use the Schur complement [25] to transform (29) into the linear matrix inequality (LMI), i.e.,

$$\begin{bmatrix} (\boldsymbol{J}_s(\boldsymbol{a_k}))^{-1} - \boldsymbol{Z}_k & \boldsymbol{I} \\ \boldsymbol{I} & \boldsymbol{J}_s(\boldsymbol{a_k}) + \boldsymbol{J}_u(\boldsymbol{a_k}) \end{bmatrix} \succeq \boldsymbol{0} \tag{30}$$

while the sum of several semidefinite matrices also satisfies

$$\frac{1}{N_k}\sum_{k=1}^{N_k} \begin{bmatrix} (\boldsymbol{J}_s(\boldsymbol{a_k}))^{-1} - \boldsymbol{Z}_k & \boldsymbol{I} \\ \boldsymbol{I} & \boldsymbol{J}_s(\boldsymbol{a_k}) + \boldsymbol{J}_u(\boldsymbol{a_k}) \end{bmatrix} \succeq \boldsymbol{0} \tag{31}$$

where $\boldsymbol{I}$ is an identity matrix with the same size as $\boldsymbol{J}_s(\boldsymbol{a_k})$.

Substituting (31) and $\boldsymbol{Z}_k \ \forall k \in \mathcal{N}_k$, into $\mathscr{P}^{\mathrm{SP}}$, the relaxed optimization problem is

$$\mathscr{P}^{\mathrm{SP-R}}: \underset{\boldsymbol{P}, \boldsymbol{Z}_1, \ldots, \boldsymbol{Z}_{N_k}}{\text{maximize}} \quad \frac{1}{N_k}\sum_{k=1}^{N_k} \mathrm{tr}\{\boldsymbol{Z}_k\} \tag{32}$$

$$\text{s.t.} \quad \text{C3, C4, and C6} \tag{33}$$

$$\text{C7: LMI in (31).} \tag{34}$$

Obviously, $\mathscr{P}^{\mathrm{SP}-R}$ is convex concerning all the decision variables so that it can be solved by using the interior-point approach.

The proposed PRTSA to solve the JPPO problem in the static SAILN is summarized in Algorithm 2. First, the PGA is used to solve the optimization problem $\mathscr{P}^S$ to obtain the candidate solution $\boldsymbol{\mathcal{X}}^c = \{\boldsymbol{P}^c, \boldsymbol{U}^c\}$, where the candidate power allocation strategy $\boldsymbol{P}^c$ is discarded and the candidate position deployment $\boldsymbol{U}^c$ is retained. Second, substituting $\boldsymbol{U}^c$ into $\mathscr{P}^{\mathrm{SP-R}}$, we can obtain the improved power allocation solution and the corresponding UAV operation strategy $\boldsymbol{\mathcal{X}}^* = \{\boldsymbol{P}^*, \boldsymbol{U}^c\}$, which is better than the candidate one.

D. Extensions to the Dynamic Network

In the dynamic SAILN, the AoI is moving, but the deployable area and the NFZ are assumed to be constant within a short period. Thus, we can obtain the deployed positions and allocated power values of UAVs using an iterative manner, i.e., step-by-step optimization. At the initial time slot, we can regard the JPPO problem as that of the static SAILN. Namely, with $\mathcal{D}$ and $\mathcal{A}[1]$, we can solve $\mathscr{P}^{\mathrm{MT}}$ by using the PRTSA to obtain $\boldsymbol{U}^c[1]$ and $\boldsymbol{P}^*[1]$. At the next time slot, $\mathcal{A}[2]$ can be derived based on the knowledge of AoI's movement and the same procedures are used to obtain $\boldsymbol{U}^c[2]$ and $\boldsymbol{P}^*[2]$. In a word, the positions and allocated power values of UAVs can be calculated by solving the optimization problem $\mathscr{P}^{\mathrm{MT}}$ at each time slot and the procedures within a period are shown in Algorithm 3.

E. Other Practical Methods

To evaluate the performance of the PGA and the PRTSA when solving our formulated problems $\mathscr{P}^{\mathrm{S}}$ and $\mathscr{P}^{\mathrm{MT}}$, we explicitly compare it with three other approaches. These three straightforward schemes perform based on the constraints and serve as the baselines, i.e., top deployment and uniform allocation (TDUA) strategy, random deployment and uniform allocation (RDUA) strategy, and random deployment and random allocation (RDRA) strategy. With the TDUA strategy, the UAVs tend to be deployed on the top of the AoI with the minimum available height, and power values are equally allocated. The deployment of UAVs can be implemented based on the following steps: 1) find the inscribed circle of a square ground projection of the AoI and 2) the x and y coordinates of UAVs are $(x_j, y_j) = \hat{\boldsymbol{o}} + \hat{r}[\cos(j*[2\pi/N_u]), \sin(j*[2\pi/N_u])]^T, j \in \mathcal{N}_u$, where $\hat{\boldsymbol{o}}$ and $\hat{r}$ are the center and radius of the inscribed circle, and the height of all the UAVs is equal to the minimum allowable value. Note that, if the position of UAV $\boldsymbol{u}_j$ is located in the NFZ, we can find the 2-D projection of $\boldsymbol{u}_j$ on the boundary along the direction determined by $\boldsymbol{u}_j$ and the center of NFZ as a substitute. With the RDUA strategy, the UAVs are deployed randomly in the deployable area, and power values are equally allocated. Specifically, the deployment can be achieved by an iterative manner: the first UAV is randomly given; the second one is generated randomly without violating the constraints of NFZ and safe distance; the remaining UAVs can be obtained by using the similar manner. Obviously, in the RDRA strategy, the UAVs are deployed randomly in the deployable area and powers are randomly allocated. In particular, the power can be allocated by $P_j \sim U(0, P_{\max})$, which may not satisfy $\sum_{j=1}^{N_u} P_j = P_{\mathrm{total}}$. The three strategies can be utilized in a static network directly and adjusted to the dynamic network when considering the related constraints.

VI. Simulations and Discussions

In this section, simulation results are given to compare the localization accuracy for the AoI provided by the SAILNs with different JPPO solutions. It is worth mentioning that the SPEBs of the sampling points in the AoI can be described by the following two manners: 1) distribution and 2) box plot. SPEB distribution depicts a set of contour lines, and SPEB box plot gives their quartiles. We first provide general network settings. Then, in a static SAILN, we evaluate the solutions of our proposed PGA and PRTSA, and the other benchmark algorithms. At last, JPPO solutions in a dynamic SAILN with multiple time slots are given and analyzed.

A. Simulation Settings

1) Position Settings: In our concerned SAILN, we focus on ground users and low-flying UAVs. Thus, the coordinates of the satellite should be converted from the well-known geodetic coordinate system (GCS), i.e., latitude, longitude, and altitude (LLA), to the local Cartesian coordinates system, i.e., east-north-up coordinate system (ENUCS). In ENUCS, we define an origin point on the ground, while x-axis points to the east, y-axis points to the north, and the z-axis points to the upward normal of the origin point. Next, we describe the detailed position settings in both static SAILN and dynamic SAILN.

In the static SAILN, there are $N_s = 3$ satellites with positions $(-4.67, 0.27, 6.94)^T$ km, $(-3.22, 0.67, 7.02)^T$ km, and $(-3.77, -0.10, 6.99)^T$ km, respectively, whose ephemeris is obtained from public satellite database. For UAVs, the deployable area $\mathcal{D}$ is a cube, i.e., $x \in [0, 3000]$ m, $y \in [0, 3000]$ m, and $z \in [200, 500]$ m, and the NFZ is a cylinder with a ground circular projection centered at $\tilde{\boldsymbol{o}} = (1000, 1000, 0)^T$ m with radius as $\tilde{r} = 500$ m, i.e., $(x-1000)+(y-1000)^2 < 500^2$. The predefined safe distance $s_{\min}$ is equal to 50 m. The ground AoI is smaller than $\mathcal{D}$ and the included range is $x \in [500, 2500]$ m, $y \in [500, 2500]$ m. The 2-D illustration of the conceived AoI and projection of NFZ on the ground is shown in Fig. 2. In the dynamic SAILN, the time interval δ_t is set to 1 s and the maximum speed of UAVs $v_{u,\max}$ is specified as 20 m/s [26]. The initial state of dynamic SAILN is the same as that of the previous static SAILN. The AoI moves along with the angle bisector of x-axis and y-axis with constant speed 10 m/s, which is estimated and known by the SAILN. Since we focus on a short period, the deployment area $\mathcal{D}$ and NFZ remain fixed and unchanged.

2) Channel Settings: For UAVs' transmission signals, the D2G path loss model and average LOS probability can refer to [26]. The maximum transmission power of UAVs is $P_{\max} = 20$ mW and the total power of all the UAVs is $P_{\mathrm{total}} = 50$ mW. The carrier frequency of ranging signal is 2.4 GHz and the bandwidth is 5 MHz [7]. Thus, ξ can be estimated and derived by the SAILN, and RIIs can be calculated according to the detailed expression in [6]. For satellites' transmission signals, we assume the RIIs $\mu_{i,k} = 2\ \forall i \in \mathcal{N}_s, k \in \mathcal{N}_k$.

3) Genetic Algorithm Settings: The population contains 50 individuals, and the maximum number of generations is set to 100. The initial chromosomes are randomly generated following uniform distribution within the feasible set. The number of reserved elites is 3, and the fraction of the crossover is 0.8. Besides, we set the tolerance of constraints to 0 and 10^{-6} in the static SAILN and the dynamic SAILN, respectively.

B. Performance Evaluations in Static SAILN

In this part, we first provide the SPEB distribution of the AoI provided by only satellites, as shown in Fig. 4. Because

TABLE I
JPPO SOLUTIONS OBTAINED BY DIFFERENT ALGORITHMS

Algorithms	Positions (km)	Power (mW)	$\mathcal{P}^A(\mathrm{m}^2)$
PGA	(2.23, 1.60, 0.37), (1.27, 2.09, 0.37), (1.48, 0.79, 0.43)	15.0, 13.0, 14.9	171.08
GAUA	(2.23, 1.60, 0.37), (1.27, 2.09, 0.37), (1.48, 0.79, 0.43)	16.7, 16.7, 16.7	171.21
PRTSA	(2.23, 1.60, 0.37), (1.27, 2.09, 0.37), (1.48, 0.79, 0.43)	11.0, 19.0, 20.0	171.25
TDUA	(1.00, 2.36, 0.20), (1.00, 0.50, 0.20), (2.50, 1.50, 0.20)	16.7, 16.7, 16.7	170.52
RDUA	(2.94, 1.63, 0.28), (2.27, 0.48, 0.33), (1.65, 0.39, 0.49)	16.7, 16.7, 16.7	168.97
RDRA	(0.74, 2.89, 0.49), (0.52, 1.61, 0.29), (2.53, 0.55, 0.37)	18.3, 16.4, 9.90	165.27

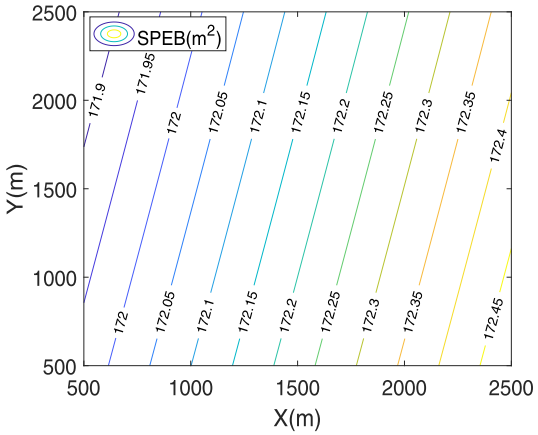

Fig. 4. Distribution of SPEB provided by only satellites.

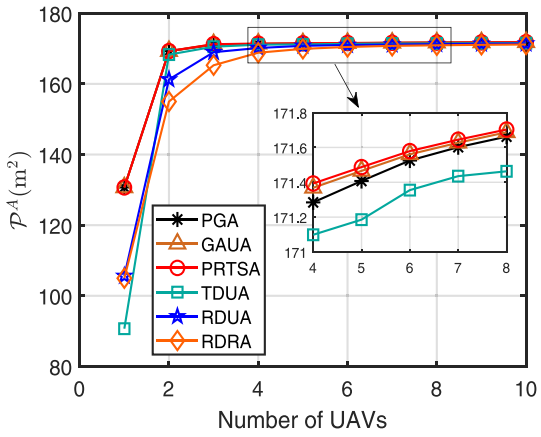

Fig. 5. ALAI versus the number of static UAVs.

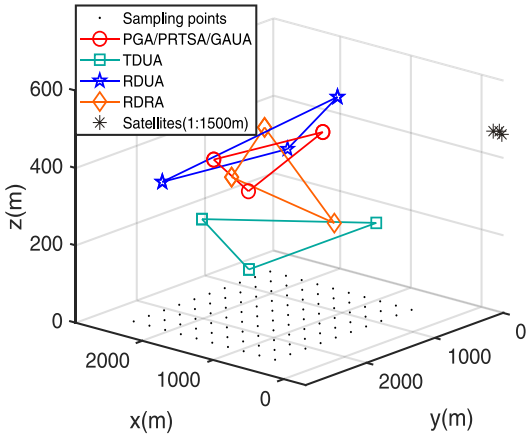

Fig. 6. 3-D positions of static UAVs.

the satellites are far away from the ground and the AoI is relatively small, the SPEBs is uniform throughout the area, i.e., the localization accuracy provided by satellites in the AoI is roughly equal to $\sqrt{172}$ m. Thus, in SAILN, the ALAI $\mathcal{P}^A$ is reasonable to be the metric to measure the increment of supplementary localization information provided by UAVs.

Fig. 5 shows the comparison of $\mathcal{P}^A$ obtained by different algorithms when the number of UAVs N_u varies from 1 to 10. Note that, the genetic algorithm and uniform allocation (GAUA) strategy is involved in verifying the function of the power reallocation. It defines a JPPO solution that the UAV positions are derived from the genetic algorithm, and the powers are uniformly allocated. Since UAVs' positions are generated randomly in the RDUA and the RDRA strategies, average $\mathcal{P}^A$ is obtained by using the Monte Carlo method with 100 trials. From the figure, we can obtain the following observations. First, compared with only satellites network, SAILN can dramatically improve the localization accuracy of the entire AoI. The ALAI becomes larger with the increase of the number of UAVs, which means that localization accuracy is improved when more UAVs are added. Second, the accuracy improvement is insignificant when the number of UAVs is more than four because the spatial positions of UAVs are close, and the total available power P_{total} is unchanged. Third, from the enlarged view, the JPPO solution obtained by the PGA performs obviously better than that of the TDUA, the RDUA, and the RDRA strategies. The ALAI determined by the JPPO solution of GAUA is larger than that of the PGA because all the available power is run out; meanwhile, the PRTSA performs better than the PGA and GAUA since the other procedures further optimize the power values.

Table I provides the detailed information of JPPO solutions obtained by different algorithms when $N_u = 3$. Besides, Figs. 6 and 7 show the corresponding 3-D and 2-D positions of UAVs. Note that the scale of satellites' positions in Fig. 6 is 1:1500 m to present the full scene of SAILN. First, the solutions obtained by all the algorithms satisfy the constraints in optimization problem $\mathscr{P}^S$, i.e., total available power, maximum available power, NFZ, and safe distance. Second, compared with the PGA, the sum of UAVs' power resolved by the GAUA and the PRTSA is equal to the total power so that these two methods can obtain a larger ALAI. Although the difference of the PGA and the PRTSA is about 0.17 m^2 (localization error ≈ 0.41 m), it has a significant impact on the autonomous driving security, disaster rescue, and other applications in smart cities. Third, it can be seen from the poor accuracy of the TDUA strategy

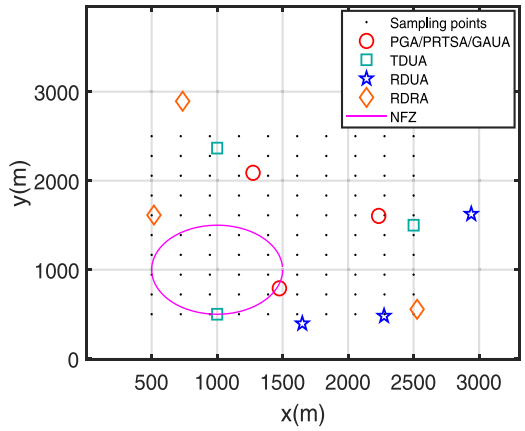

Fig. 7. 2-D positions of static UAVs.

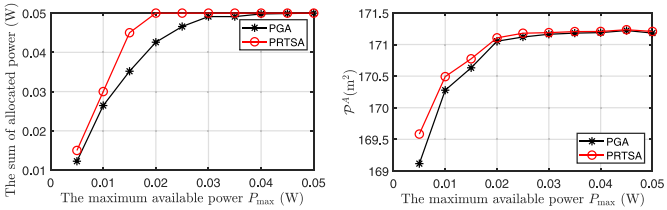

Fig. 8. Comparison of PGA and PRTSA when $P_{\max}$ varies. (a) $\|\boldsymbol{P}\|_1$ versus $P_{\max}$. (b) $\mathcal{P}^A$ versus $P_{\max}$.

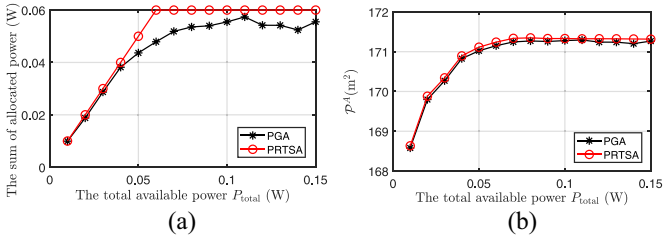

Fig. 9. Comparison of PGA and PRTSA when P_{total} varies. (a) $\|\boldsymbol{P}\|_1$ versus P_{total}. (b) $\mathcal{P}^A$ versus P_{total}.

that when considering the AoI and the D2G channel model, the optimal flying height of the UAVs is not the lowest one.

Then, with $N_u = 3$, we compare the power allocation solutions of the PGA and the PRTSA as $P_{\max}$ and P_{total} varying in the constraints. On one hand, when the total available power P_{total} is equal to 50 mW, Fig. 8 shows the comparison of the PGA and the PRTSA, i.e., ALAI $\mathcal{P}^A$ versus $P_{\max}$ and the sum of allocated power $\|\boldsymbol{P}\|_1$ versus $P_{\max}$, where $\|\cdot\|_1$ denotes the ℓ_1 norm. It is obvious that a better power allocation strategy should run out of all the available power, to obtain a better localization accuracy. In Fig. 8(a), when $P_{\max}$ is larger than 20mW, it satisfies $N_u \times P_{\max} > P_{\text{total}}$. Obviously, $\|\boldsymbol{P}\|_1$ solved by the PRTSA reaches the upper bound P_{total}, but the PGA method is incapable. Thus, a larger ALAI $\mathcal{P}^A$ is obtained by the PRTSA in Fig. 8(b). On the other hand, when the maximum allowable power $P_{\max}$ is equal to 20 mW, Fig. 9 shows the comparison of the PGA and the PRTSA when P_{total} vaires. In Fig. 9(a), $\|\boldsymbol{P}\|_1$ solved by the PRTSA is equal to P_{total} before $P_{\text{total}} = 60$mW, and stays fixed as the P_{total} incresing. In contrast, $\|\boldsymbol{P}\|_1$ solved by the PGA is always lower than that of the PRTSA, so that a worse localization accuracy is obtained, shown in Fig. 9(b). In summary, the expected drawback of the PGA is that the sum of the allocated power cannot reach the total power, which can be compensated by the PRTSA by reaping the power reallocation.

When the JPPO solutions in Table I are used to form SAILN, the SPEB distributions for the entire AoI are depicted in Fig. 10(a)–(e), and the box plot of different algorithms is shown in Fig. 10(f). From this set of figures, we have the following observations. First, the center subarea of the AoI has a better localization accuracy than the edge subarea since the UAVs tend to deploy on the top of the AoI (known from Fig. 7) to obtain a better elevation angle and a larger RII $\mu_{j,k}$ in (6). Second, it is obvious that the subarea surrounded by the 0.5 m^2-contour line in Fig. 10(b) is wider than that of Fig. 10(a), which can verify again that the PRTSA is superior to the PGA. In Fig. 10(f), we can obtain the same conclusion by comparing the quartiles and outliers of the SPEBs of all the sampling points. Third, the proposed optimization framework gives a reference for the expected localization accuracy. For example, to achieve a level accuracy of around $\sqrt{0.5}$ m, at least three UAVs should be deployed according to the obtained JPPO solution.

C. Effect of UAVs' Position Uncertainties in Static SAILN

Although different algorithms can determine the approximately optimal JPPO solutions, the UAVs' self-localization error makes them unable to move to the obtained position accurately. In the considered scenario, the UAVs' self-localization error is called as position uncertainties. In this part, we verify the negative effect of the position uncertainties on the localization accuracy of the AoI.

We still use the obtained JPPO solutions in Table I to complete the performance comparison, where the number of UAVs $N_u = 3$. Then, the random uncertainties are added to the UAVs' positions obtained by different algorithms, and the uncertainties follow the uniform distribution and Gaussian distribution, respectively. For instance, denoting by $\boldsymbol{U}^o_{\text{PGA}}$ the UAVs' position vector determined by the PGA, the actual UAVs' position vector is $\boldsymbol{U}_{\text{PGA}} = \boldsymbol{U}^o_{\text{PGA}} + \boldsymbol{E}_{\text{PGA}}$, where $\boldsymbol{E}_{\text{PGA}} \sim U(-\sigma, \sigma)$ (Uniform distribution) or $\boldsymbol{E}_{\text{PGA}} \sim N(0, \sigma^2)$ (Gaussian distribution) is the position uncertainties vector. In our simulation, the standard deviation σ varies from 0 to 100. The metric to scale the localization accuracy of the AoI in the presence of random UAVs' positions uncertainties is the average ALAI, which can be obtained by using the Monte Carlo method with 500 trials. Note that, in each trial, it is indispensable to examine whether the solution violating the constraints C1 and C2 in problem $\mathscr{P}^{\text{S}}$.

Figs. 11 and 12 show the average ALAI obtained by different algorithms with varying standard deviation of UAVs' position uncertainties, which follow the uniform distribution and Gaussian distribution, respectively. First, no matter what the distribution of uncertainties is, the average ALAI decreases monotonically with σ, which means the localization accuracy for the AoI deteriorates as the UAVs position uncertainties increase. Therefore, to minimize the localization error for the

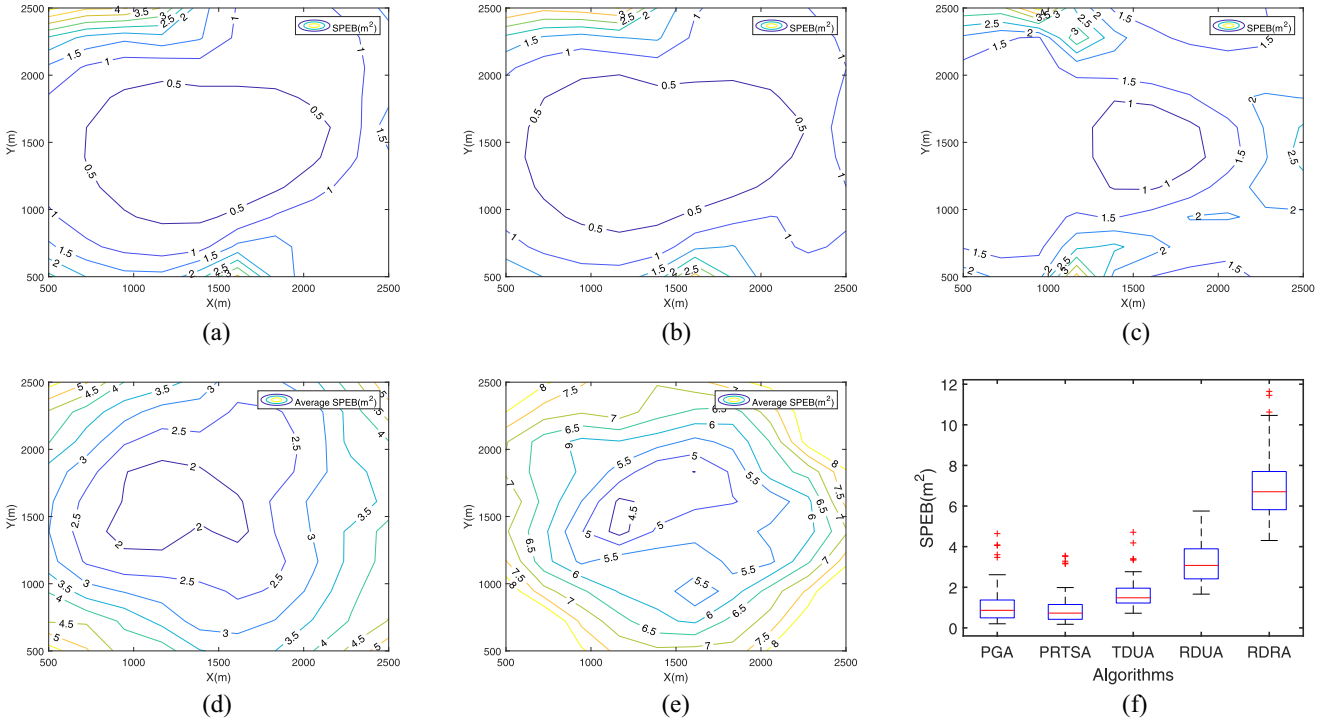

Fig. 10. SPEB distributions of the AoI provided by the static SAILN when using different JPPO algorithms.

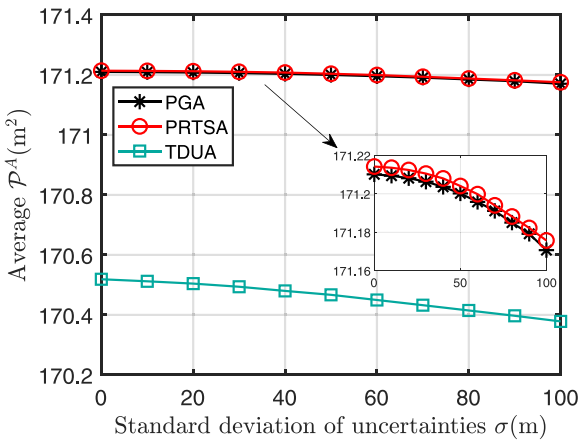

Fig. 11. Average ALAI obtained by different algorithms versus UAVs' position uncertainties (Uniform Distribution).

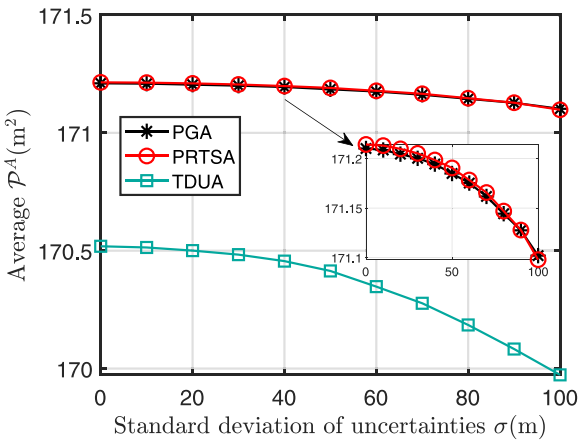

Fig. 12. Average ALAI obtained by different algorithms versus UAVs' position uncertainties (Gaussian Distribution).

IoT devices in the AoI, the UAVs need to improve their self-localization accuracy and accurately move to the position obtained by the JPPO algorithms. Second, compared with the TDUA method, even when the UAVs' position uncertainties are large, the average ALAI determined by the PRTSA is very close to that without the uncertainties. Therefore, the proposed PRTSA is robust in the presence of the UAVs' position uncertainties and can be realized in the real world.

D. JPPO Results in Dynamic SAILN

We then consider the dynamic SAILN with multiple time steps. The initial positions of three satellites are the same as those given in the previous simulation, and their movement is based on preset orbit and ephemeris. For different algorithms, the initial conditions of the UAVs are determined by implementing themselves in the initial static SAILN. In this part, the RDUA and the RDRA strategies are unconsidered since the speed constraint of UAVs in two successive time steps may be unsatisfied when using these two methods. The TDUA can be implemented in each time step due to the movement of AoI is slower than the UAVs.

When the number of UAVs $N_u = 3$ and $N_u = 5$, Fig. 13 shows the comparison of $\mathcal{P}^A$ obtained by the PGA, the PRTSA, and the TDUA within a period with $N_t = 15$ time steps. Since the ALAI of the PGA and the PRTSA are very close, the performance gap $\mathcal{P}^A_{\text{PRTSA}} - \mathcal{P}^A_{\text{PGA}}$ is depicted in Fig. 14. From these two figures, we can obtain the following observations. First, the PGA and the PRTSA can obtain larger objective values than the TDUA strategy during the entire period. Second, the performance gap $\mathcal{P}^A_{\text{PRTSA}} - \mathcal{P}^A_{\text{PGA}}$

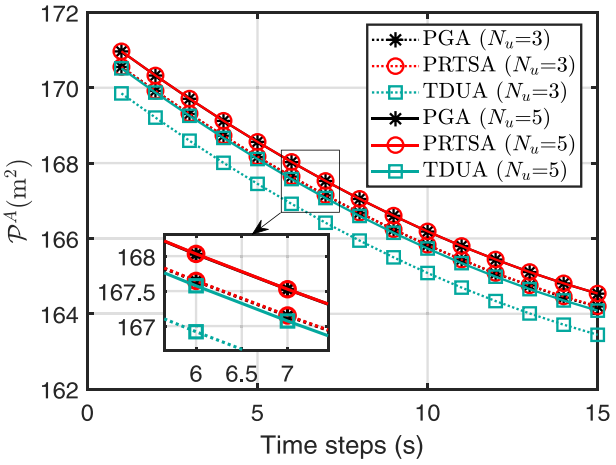

Fig. 13. ALAI solved by different algorithms versus time steps.

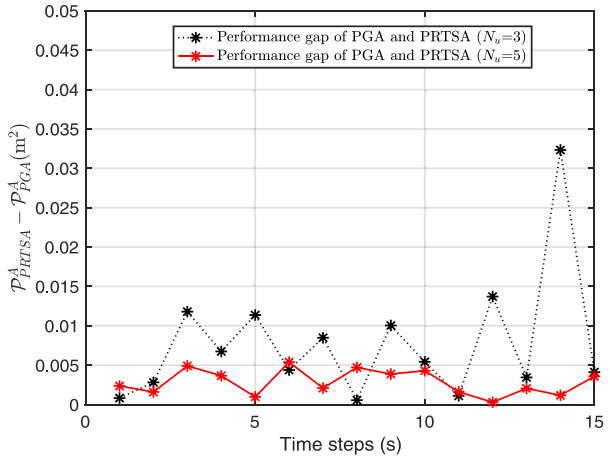

Fig. 14. ALAI gap of PGA and PRTSA algorithms.

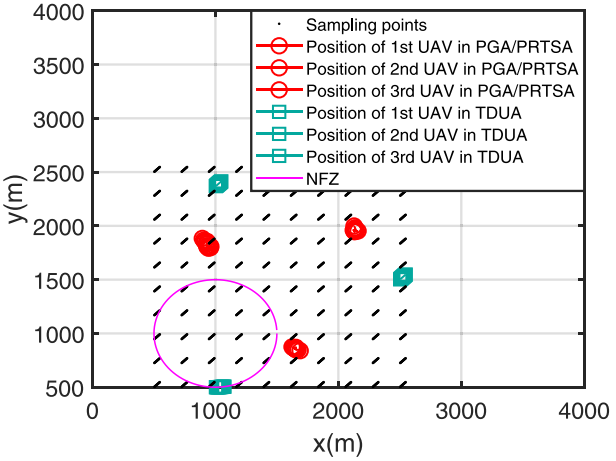

Fig. 15. UAVs' 2-D positions obtained by different algorithms.

is always positive, which demonstrates that the PRTSA performs better than the PGA. Third, comparing the solid and dash lines, a higher ALAI can be obtained when more UAVs are added in the SAILN. Fourth, the performance curves of the PGA and the PRTSA with $N_u = 3$ are superior to that of the TDUA when $N_u = 5$, which means that a good JPPO solution improves the localization accuracy for the AoI while reduces the number of added UAVs.

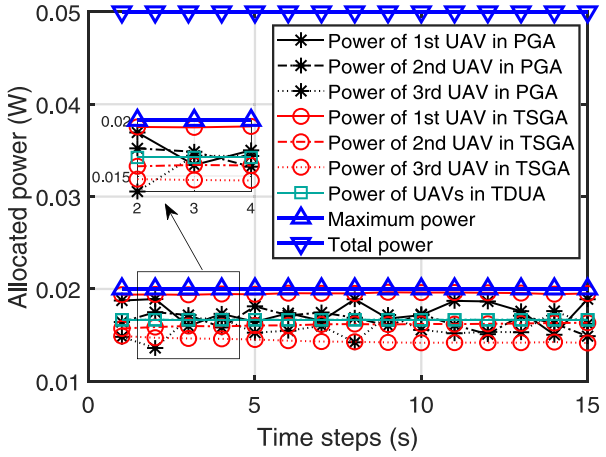

Fig. 16. UAVs' power allocated by different algorithms.

When the number of UAVs N_u is equal to 3, Fig. 15 shows the 2-D trajectories of each UAV determined by the PGA/PRTSA and the TDUA strategy, respectively. Each sampling point in the AoI becomes a short line because the AoI moves along the angle bisector of x-axis and y-axis, while the NFZ and deployment area are fixed. Meanwhile, Fig. 16 depicts the allocated power values of the PGA, the PRTSA, and the TDUA. From these two figures, we can obtain the following observations. First, each UAV trajectory is relatively concentrated due to the speed constraint in two successive time steps. Second, the positions of all UAVs are out of the NFZ and distance between every two UAVs is larger than the safe distance. Third, the allocated power of every UAV is lower than the maximum allowable value.

VII. Conclusion

In this article, we have investigated the JPPO of UAVs in SAILN to minimize the localization error of the entire AoI. We have formulated the JPPO problems in both static and dynamic SAILNs by regarding the ALAI as the localization accuracy metric of the AoI. Because of the intractability of deriving an analytical solution, the PGA and PRTSA algorithms have been proposed to resolve the nonconvex JPPO problems. Simulation results have demonstrated that the PGA and the PRTSA algorithms perform better than the three baseline methods, and the PRTSA is insensitive to the UAVs' position uncertainties. Our work can offer valuable insights into the important yet unexplored field of regional localization in SAILN.

For our future work, we will further investigate the impact of the synchronization errors, correlation of UAVs position and pseudoranges, and channel parameter uncertainty on the localization performance of SAILN.

References

[1] S. Kuutti, S. Fallah, K. Katsaros, M. Dianati, F. Mccullough, and A. Mouzakitis, "A survey of the state-of-the-art localization techniques and their potentials for autonomous vehicle applications," *IEEE Internet Things J.*, vol. 5, no. 2, pp. 829–846, Apr. 2018.

[2] M. S. Mahmud, H. Fang, and H. Wang, "An integrated wearable sensor for unobtrusive continuous measurement of autonomic nervous system," *IEEE Internet Things J.*, vol. 6, no. 1, pp. 1104–1113, Feb. 2019.

[3] J. Zhang, R. Liu, K. Yin, Z. Wang, M. Gui, and S. Chen, "Intelligent collaborative localization among air-ground robots for industrial environment perception," *IEEE Trans. Ind. Electron.*, vol. 66, no. 12, pp. 9673–9681, Dec. 2019.
[4] Z. Hu, Z. Bai, K. Bian, T. Wang, and L. Song, "Real-time fine-grained air quality sensing networks in smart city: Design, implementation, and optimization," *IEEE Internet Things J.*, vol. 6, no. 5, pp. 7526–7542, Oct. 2019.
[5] M. Modsching, R. Kramer, and K. Hagen, "Field trial on GPS accuracy in a medium size city: The influence of built-up," in *Proc. 3rd Workshop Position. Navig. Commun.*, 2006, pp. 209–218.
[6] Y. Shen and M. Z. Win, "Fundamental limits of wideband localization—Part I: A general framework," *IEEE Trans. Inf. Theory*, vol. 56, no. 10, pp. 4956–4980, Oct. 2010.
[7] Y. Liu and Y. Shen, "UAV-aided high-accuracy relative localization of ground vehicles," in *Proc. IEEE Int. Conf. Commun. (ICC)*, Kansas City, MO, USA, 2018, pp. 1–6.
[8] M. Mozaffari, W. Saad, M. Bennis, and M. Debbah, "Mobile unmanned aerial vehicles (UAVs) for energy-efficient Internet of Things communications," *IEEE Trans. Wireless Commun.*, vol. 16, no. 11, pp. 7574–7589, Nov. 2017.
[9] G. Ding, Q. Wu, L. Zhang, Y. Lin, T. A. Tsiftsis, and Y. Yao, "An amateur drone surveillance system based on the cognitive Internet of Things," *IEEE Commun. Mag.*, vol. 56, no. 1, pp. 29–35, Jan. 2018.
[10] J. Liu, Y. Shi, Z. M. Fadlullah, and N. Kato, "Space-air-ground integrated network: A survey," *IEEE Commun. Surveys Tuts.*, vol. 20, no. 4, pp. 2714–2741, 4th Quart., 2018.
[11] N. Zhang, S. Zhang, P. Yang, O. Alhussein, W. Zhuang, and X. Shen, "Software defined space-air-ground integrated vehicular networks: Challenges and solutions," *IEEE Commun. Mag.*, vol. 55, no. 7, pp. 101–109, Jul. 2017.
[12] N. Cheng *et al.*, "Space/aerial-assisted computing offloading for IoT applications: A learning-based approach," *IEEE J. Sel. Areas Commun.*, vol. 37, no. 5, pp. 1117–1129, May 2019.
[13] A. Danjo, Y. Watase, and S. Hara, "A theoretical error analysis on indoor TOA localization scheme using unmanned aerial vehicles," in *Proc. IEEE 81st Veh. Technol. Conf. (VTC Spring)*, Glasgow, U.K., 2015, pp. 1–5.
[14] N. Cheng *et al.*, "A comprehensive simulation platform for space-air-ground integrated network," *IEEE Wireless Commun.*, vol. 27, no. 1, pp. 178–185, Feb. 2020.
[15] A. A. Khuwaja, Y. Chen, N. Zhao, M. Alouini, and P. Dobbins, "A survey of channel modeling for UAV communications," *IEEE Commun. Surveys Tuts.*, vol. 20, no. 4, pp. 2804–2821, 4th Quart., 2018.
[16] Y. Liu, Z. Qin, Y. Cai, Y. Gao, G. Y. Li, and A. Nallanathan, "UAV communications based on non-orthogonal multiple access," *IEEE Wireless Commun.*, vol. 26, no. 1, pp. 52–57, Feb. 2019.
[17] W. Wang *et al.*, "Joint precoding optimization for secure SWIPT in UAV-aided NOMA networks," *IEEE Trans. Commun.*, vol. 68, no. 8, pp. 5028–5040, Aug. 2020.
[18] Q. Wu, L. Liu, and R. Zhang, "Fundamental trade-offs in communication and trajectory design for UAV-enabled wireless network," *IEEE Wireless Commun.*, vol. 26, no. 1, pp. 36–44, Feb. 2019.
[19] Y. Shen and M. Z. Win, "Energy efficient location-aware networks," in *Proc. IEEE Int. Conf. Commun. (ICC)*, Beijing, China, 2008, pp. 2995–3001.
[20] M. Z. Win, W. Dai, Y. Shen, G. Chrisikos, and H. V. Poor, "Network operation strategies for efficient localization and navigation," *Proc. IEEE*, vol. 106, no. 7, pp. 1224–1254, Jul. 2018.
[21] B. Yang, "Different sensor placement strategies for TDOA based localization," in *Proc. IEEE Int. Conf. Acoust. Speech Signal Process. (ICASSP)*, Honolulu, HI, USA, 2007, pp. 1093–1096.
[22] B. Yang and J. Scheuing, "Cramer-rao bound and optimum sensor array for source localization from time differences of arrival," in *Proc. IEEE Int. Conf. Acoust. Speech Signal Process. (ICASSP)*, Philadelphia, PA, USA, 2005, pp. 961–964.
[23] N. H. Nguyen and K. Doğançay, "Optimal geometry analysis for multistatic TOA localization," *IEEE Trans. Signal Process.*, vol. 64, no. 16, pp. 4180–4193, Aug. 2016.
[24] S. Xu and K. Doğançay, "Optimal sensor placement for 3-D angle-of-arrival target localization," *IEEE Trans. Aerosp. Electron. Syst.*, vol. 53, no. 3, pp. 1196–1211, Jun. 2017.
[25] Y. Zhao, Z. Li, B. Hao, and J. Shi, "Sensor selection for TDOA-based localization in wireless sensor networks with non-line-of-sight condition," *IEEE Trans. Veh. Technol.*, vol. 68, no. 10, pp. 9935–9950, Oct. 2019.
[26] W. Shi *et al.*, "Multi-drone 3-D trajectory planning and scheduling in drone-assisted radio access networks," *IEEE Trans. Veh. Technol.*, vol. 68, no. 8, pp. 8145–8158, Aug. 2019.
[27] H. Berns, T. Burnett, R. Gran, and R. Wilkes, "GPS time synchronization in school-network cosmic ray detectors," *IEEE Trans. Nucl. Sci.*, vol. 51, no. 3, pp. 848–853, Jun. 2004.
[28] H. Berns and R. Wilkes, "GPS time synchronization system for K2K," *IEEE Trans. Nucl. Sci.*, vol. 47, no. 2, pp. 340–343, Apr. 2000.
[29] Z. Li *et al.*, "Multiobjective optimization based sensor selection for TDOA tracking in wireless sensor network," *IEEE Trans. Veh. Technol.*, vol. 68, no. 12, pp. 12360–12374, Dec. 2019.
[30] T.-Y. Lin, K.-C. Hsieh, and H.-C. Huang, "Applying genetic algorithms for multiradio wireless mesh network planning," *IEEE Trans. Veh. Technol.*, vol. 61, no. 5, pp. 2256–2270, Jun. 2012.
[31] B. Lorenzo and G. Savo, "Optimal routing and traffic scheduling for multihop cellular networks using genetic algorithm," *IEEE Trans. Mobile Comput.*, vol. 12, no. 11, pp. 2274–2288, Nov. 2013.
[32] R. L. Haupt and S. E. Haupt, *Practical Genetic Algorithms*. Hoboken, NJ, USA: Wiley, 2004.
[33] K. Deb, "An efficient constraint handling method for genetic algorithms," *Comput. Methods Appl. Mech. Eng.*, vol. 186, pp. 311–338, Jun. 2000.
[34] D. J. Reid, "Genetic algorithms in constrained optimization," *Math. Comput. Model.*, vol. 23, no. 5, pp. 87–111, Jun. 1996.
[35] A. Konak, D. W. Coit, and A. E. Smith, "Multi-objective optimization using genetic algorithms: A tutorial," *Rel. Eng. Syst. Safety*, vol. 91, no. 9, pp. 992–1007, Sep. 2006.

Yue Zhao (Member, IEEE) received the Ph.D. degree from the School of Telecommunications Engineering, Xidian University, Xi'an, China, in 2020.

He is currently an Associate Professor with the State Key Laboratory of Integrated Services Networks, School of Telecommunication Engineering, Xidian University. From 2018 to 2019, he was a visiting student with the Broadband Communications Research Group, Department of Electrical and Computer Engineering, University of Waterloo, Waterloo, ON, Canada. His research interests include space-air-ground integrated network, wireless network localization, and covert communications.

Zan Li (Senior Member, IEEE) received the B.S. degree in communications engineering and the M.S. and Ph.D. degrees in communication and information systems from Xidian University, Xi'an, China, in 1998, 2001, and 2006, respectively.

She is currently a Professor with the State Key Laboratory of Integrated Services Networks, School of Telecommunications Engineering, Xidian University. Her research interests include topics on wireless communications and signal processing, such as covert communication, spectrum sensing, and cooperative communications.

Prof. Li was awarded the National Natural Science Fund for Distinguished Young Scholars. She is a Fellow of Institution of Engineering and Technology, China Institute of Electronics, and China Institute of Communications. She serves as an Associate Editor for the IEEE TRANSACTIONS ON COGNITIVE COMMUNICATIONS AND NETWORKING and *China Communications*.

Nan Cheng (Member, IEEE) received the B.E. and M.S. degrees from the Department of Electronics and Information Engineering, Tongji University, Shanghai, China, in 2009 and 2012, respectively, and the Ph.D. degree from the Department of Electrical and Computer Engineering, University of Waterloo, Waterloo, ON, Canada, in 2016.

He is currently a Professor with the State Key Laboratory of Integrated Services Networks, School of Telecommunication Engineering, Xidian University, Xi'an, China. He worked as a Postdoctoral Fellow with the Department of Electrical and Computer Engineering, University of Toronto, Toronto, ON, Canada, from 2017 to 2018. His current research focuses on space-air-ground integrated system, big data in vehicular networks, and self-driving system. His research interests also include performance analysis, MAC, opportunistic communication, and application of AI for vehicular networks.

Benjian Hao (Member, IEEE) received the B.S. degree in electronic and information engineering, the M.S. degree (First Class Hons.) in communication and information systems, and the Ph.D. degree in communication and information systems from Xidian University, Xi'an, China, in 2006, 2009, and 2013, respectively.

From 2014 to 2016, he was a lecturer with Xidian University. From October 2017 to November 2018, he was a Visiting Scholar with the University of Missouri, Columbia, MO, USA. He is currently an Associate Professor with the State Key Laboratory of Integrated Services Networks, Xidian University. His research interests include source localization, sensor array processing, spectrum sensing and signal detection, signal identification, and wireless communications.

Xuemin (Sherman) Shen (Fellow, IEEE) received the Ph.D. degree in electrical engineering from Rutgers University, New Brunswick, NJ, USA, in 1990.

He is currently a University Professor with the Department of Electrical and Computer Engineering, University of Waterloo, Waterloo, ON, Canada. His research focuses on resource management in interconnected wireless/wired networks, wireless network security, social networks, smart grid, and vehicular *ad hoc* and sensor networks.

Dr. Shen received the R.A. Fessenden Award in 2019 from IEEE, Canada, Award of Merit from the Federation of Chinese Canadian Professionals (Ontario) presents in 2019, James Evans Avant Garde Award in 2018 from the IEEE Vehicular Technology Society, Joseph LoCicero Award in 2015 and Education Award in 2017 from the IEEE Communications Society, and Technical Recognition Award from Wireless Communications Technical Committee in 2019 and AHSN Technical Committee in 2013. He has also received the Excellent Graduate Supervision Award in 2006 from the University of Waterloo and the Premier's Research Excellence Award in 2003 from the Province of Ontario, Canada. He served as the Technical Program Committee Chair/Co-Chair for the IEEE Globecom'16, the IEEE Infocom'14, the IEEE VTC'10 Fall, the IEEE Globecom'07, the Symposia Chair for the IEEE ICC'10, and the Chair for the IEEE Communications Society Technical Committee on Wireless Communications. He is the elected IEEE Communications Society Vice President for Technical & Educational Activities, the Vice President for Publications, the Member-at-Large on the Board of Governors, the Chair of the Distinguished Lecturer Selection Committee, a Member of IEEE Fellow Selection Committee. He was/is the Editor-in-Chief of the IEEE INTERNET OF THINGS JOURNAL, IEEE NETWORK, *IET Communications*, and *Peer-to-Peer Networking and Applications*. He is a registered Professional Engineer of Ontario, Canada, an Engineering Institute of Canada Fellow, a Canadian Academy of Engineering Fellow, a Royal Society of Canada Fellow, a Chinese Academy of Engineering Foreign Fellow, and a Distinguished Lecturer of the IEEE Vehicular Technology Society and Communications Society.